Spectroscopic Characterization of Structural Isomers of Naphthalene: (*E*)- and (*Z*)-Phenylvinylacetylene†

Ching-Ping Liu,‡ Josh J. Newby, Christian W. Müller, Hsiupu D. Lee, and Timothy S. Zwier*

Department of Chemistry, Purdue University, West Lafayette, Indiana 47907-2084

Received: April 15, 2008; Revised Manuscript Received: June 2, 2008

Near-pure samples of (*E*)-phenylvinylacetylene ((*E*)-PVA) and (*Z*)-phenylvinylacetylene ((*Z*)-PVA) were synthesized, and their ultraviolet spectroscopy was studied under jet-cooled conditions. The fluorescence excitation and UV−UV holeburning (UVHB) spectra of both isomers were recorded. The S_0-S_1 origin of (*E*)-PVA occurs at 33 578 cm^{-1}, whereas that for (*Z*)-PVA occurs at 33 838 cm^{-1}, 260 cm^{-1} above that for (*E*)-PVA. The present study focuses primary attention on the vibronic spectroscopy of (*E*)-PVA. Single vibronic level fluorescence spectra of many prominent bands in the first 1200 cm^{-1} of the S_0-S_1 excitation spectrum of (*E*)-PVA were recorded, including several hot bands involving low-frequency out-of-plane vibrations. Much of the ground-state vibronic structure observed in these spectra was assigned by comparison with styrene and *trans*-β-methylstyrene, assisted by calculations at the DFT B3LYP/6-311++G(d,p) level of theory. Both S_0 and S_1 states of (*E*)-PVA are shown to be planar, with intensity appearing only in even overtones of out-of-plane vibrations. Due to its longer conjugated side chain compared with that of its parent styrene, (*E*)-PVA supports extensive Duschinsky mixing among the four lowest-frequency out-of-plane modes ($\nu_{45}-\nu_{48}$), increasing the complexity of this mixing relative to that of styrene. Identification of the $v'' = 0-3$ levels of ν_{48}, the lowest frequency torsion, provided a means of determining the 1D torsional potential for hindered rotation about the $C_{ph}-C_{vinyl}$ bond. Vibronic transitions due to (*Z*)-PVA were first identified as small vibronic bands that did not appear in the UVHB spectrum recorded with the hole-burn laser fixed on the S_0-S_1 origin of (*E*)-PVA. The LIF and UVHB spectra of a synthesized sample of (*Z*)-PVA confirmed this assignment.

I. Introduction

In circumstances ranging from combustion to planetary atmospheres, the appearance of $m/z = 128$ products in mass spectra are commonly attributed to naphthalene ($C_{10}H_8$, $M = 128$ g/mol).[1–4] However, there are many stable $C_{10}H_8$ isomers whose possible formation render the standard assumption of naphthalene formation doubtful and in need of experimental verification. As a result, the spectroscopic characterization of other $C_{10}H_8$ structural isomers, such as the ethynylstyrenes (*o*-, *m*-, and *p*-ES), and phenylvinylacetylene (PVA, 1-phenyl-1-buten-3-yne), is important to an understanding of the photochemical or combustion pathways leading to the formation of polyaromatic hydrocarbons (PAHs). Previous photochemical investigations in our group identified two $C_{10}H_8$ products, *m*-ES and PVA, resulting from the reaction of UV-excited diacetylene with ground state ($\tilde{X}^1A'$) styrene.[5] We have recently studied the conformation-specific spectroscopy of *o*-, *m*-, and *p*-ES and determined the cis−trans energy differences and barriers to conformational isomerization of *m*-ES in its S_0 state.[6,7] PVA, however, was not characterized spectroscopically in any further detail beyond its mere identification as one of the photoproducts of C_4H_2* + styrene.

In this work, we undertake a more complete characterization of the ultraviolet spectroscopy of PVA to determine the spectroscopic signatures of its *E*- and *Z*-isomers. This is a necessary first step in their identification as intermediates leading to naphthalene and higher-order PAHs in Titan's atmosphere, sooting flames, discharges, and interstellar media. The present study also served to identify PVA as one of the previously unassigned products with $m/z = 128$ ($C_{10}H_8$) formed in the benzene discharge studied by Güthe et al.[8,9] (see Figure 4b of ref 8).

PVA is a close structural analog of styrene, extending its conjugated vinyl substituent with an ethynyl group. By virtue of its prototypical character as a phenyl derivative with a conjugated substituent, styrene has been the subject of numerous experimental and theoretical studies.[10–16]

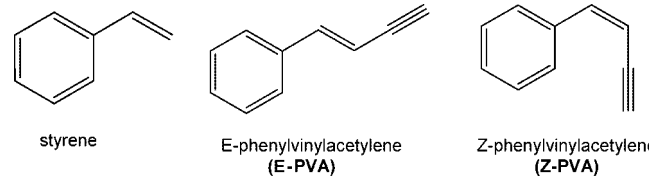

The $S-S_1$ transition in styrene is a $\pi-\pi^*$ transition that changes the bond order in the phenyl ring, vinyl group, and the connecting $C_\phi-C(\alpha)$ bond. The vibronic progressions accompanying this transition reflect the geometry changes induced by electronic excitation and have been used to deduce the magnitude and nature of these structural modifications.[17,18]

The phenyl−vinyl torsional progression is readily observed in the single vibronic level fluorescence spectrum, serving as a testing ground to assess whether a one-dimensional, symmetric torsional potential will adequately describe it. Furthermore, the form of the normal modes can also change from one electronic state to another, an effect known as Duschinsky rotation or

† Part of the "Stephen R. Leone Festschrift".

* Author to whom correspondence should be addressed. E-mail: zwier@purdue.edu

‡ Present address: Department of Biological Science and Technology, National Chiao Tung University, Hsinchu, 30050 Taiwan

10.1021/jp803254d CCC: $40.75
Published on Web 08/12/2008

Duschinsky mixing.[19] These effects have been studied in extensive detail in styrene.[10–12,15,16,20–23] In particular, Duschinsky mixing between the C(1)−C(α) torsional and out-of-plane butterfly modes has received appreciable experimental and theoretical attention in the past, rendering styrene as a prototypical example of Duschinsky mixing between two out-of-plane vibrational coordinates.[11,13,21,24,25] In PVA, the longer conjugated side chain can give rise to enhanced Duschinsky mixing between several out-of-plane S_1 coordinates because of sizable bond order changes that accompany electronic excitation.

Since ES and PVA share the same molecular formula as naphthalene, either of these isomers could undergo unimolecular isomerization to naphthalene; however, ring closure would seem most likely in *cis-o*-ES and (*Z*)-PVA, in which the side chains are in more favorable configurations. The ground-state pathway from *cis-o*-ES to naphthalene has been explored theoretically by Hopf and co-workers.[26] Unfortunately, *cis-o*-ES was not observed in a previous jet study, and therefore, the isomerization has not been investigated experimentally.[27] This paper concentrates on the spectroscopy of the *E*-isomer of PVA. However, during the course of this study, we have discovered transitions due to the *Z*-isomer as weak, unaccounted for transitions in the spectrum of (*E*)-PVA. The LIF excitation spectrum of a synthesized sample of (*Z*)-PVA proves it as the source of this spectrum, providing an important first step toward its more complete spectroscopic characterization and serving as a foundation for future studies of the photoisomerization of these $C_{10}H_8$ isomers between one another and to naphthalene.

II. Methods

A. Experimental Details. The experimental setup is similar to that described previously.[6,30] Briefly, the sample was seeded into helium at room temperature before expansion through a pulsed nozzle (General valve series 9, orifice diameter 0.8 mm). The stagnation pressure was typically 3.6 bar helium, and the flow rates were ~0.67 bar cm^3 sec^{-1}, which led to a background pressure of $\sim 2 \times 10^{-3}$ mbar inside the vacuum chamber.

The fluorescence excitation spectrum and single vibronic level fluorescence (SVLF) spectra were acquired using a new chamber equipped with two 4-in. spherical mirrors designed to increase the efficiency of fluorescence collection.[6,30] In the fluorescence experiments, the $S_1 \leftarrow S_0$ transitions were excited with the output of a frequency-doubled dye laser (Radiant Dyes NarrowScan) pumped by a Nd:YAG laser (InnoLas Spitlight 600) operating at 20 Hz. Rhodamine 6G, 610, and their mixture were used to probe the spectral region between 282 and 298 nm. Typically, <0.1 mJ/pulse of UV laser energy was used to minimize saturation effects in the excitation spectrum.

Fluorescence excitation spectra were recorded by collecting the total fluorescence through a WG 305 cutoff filter and detecting it by a UV-sensitive photomultiplier tube. The fluorescence intensity was normalized for the variation of laser power with respect to wavelength. Signals were averaged by a fast digital oscilloscope (Tektronix model 3025B) and then processed and recorded on a personal computer. For the SVLF experiments, the fluorescence was collected and focused by a plano-convex lens onto the entrance slit (50 μm) of a 0.75 m monochromator (JY750i, 2400 grooves/mm). The monochromator was equipped with a CCD camera (Andor series DU440BT) at the exit port. The relative timing between the pulsed valve, the laser system, and the data acquisition system was controlled with a digital delay generator (Berkeley Nucleonic model, BNC 555).

For the R2PI experiments, the $S_1 \leftarrow S_0$ transitions were excited with the frequency-doubled radiation of a commercial dye laser (Lambda Physik, Scanmate 2E) pumped by a Nd:YAG laser (Continuum, LU661) operating at 20 Hz. Ions produced by the two-photon absorption were accelerated into a time-of-flight mass spectrometer and detected by a microchannel plate ion detector. The ion signal was amplified 25 times (Stanford Research System model SR445) and averaged by a fast oscilloscope.

The excitation spectra possess transitions due to all conformational and structural isomers present in the expansion-cooled mixture. UV−UV hole-burning spectroscopy (UVHB) was, therefore, used to determine the number of isomers and obtain their individual UV spectral signatures. For the UVHB experiments, a tunable dye laser operating at 10 Hz was fixed on a particular $S_1 \leftarrow S_0$ vibronic transition in the excitation spectrum. The power of this hole-burning laser (0.5 mJ/pulse) was sufficient to partially saturate the transition. A probe laser was spatially overlapped with the holeburn laser and delayed from it by ~100 ns. The probe laser (20 Hz) was tuned across the $S_1 \leftarrow S_0$ vibronic transitions of interest. When the probe laser was resonant with a transition that shared the same ground-state level as the transition on which the holeburn laser was set, depletion of the ground-state population was detected by the probe laser. The difference between the signal with and without the holeburn laser present was monitored via active baseline subtraction with a Boxcar gated integrator.

Phenylvinylacetylene was synthesized at Purdue University according to a published procedure.[31] Helium (99.995%) was used as a buffer gas.

B. Computational Details. Assignment of the spectra was assisted by calculations using the Gaussian 03 suite of programs.[32] Density functional theory (DFT) calculations using the Becke3LYP functional[33,34] and the 6-311++G(d,p)[35–37] basis set were used to determine optimized geometries, energies, and harmonic frequencies. True conformational minima were verified by the lack of imaginary frequencies in the harmonic frequency calculations. Configuration interaction single (CIS) calculations[38] with the 6-311++G(d,p) basis set were performed to obtain the optimized excited-state geometries and excited-state vibrational frequencies. The computational resources of GridChem were employed due to the high computational cost of CIS calculations.[39,40]

Potential energy curves along the torsional coordinate in the S_0 state as a function of the torsional dihedral angle $\phi = \angle(2, 1, \alpha, \beta)$ (for atom labeling scheme, see Figure 1) were calculated. Relaxed potential energy scans, which represent the adiabatic rotation of the phenyl and vinylacetylenic moieties against each other, were carried out by increasing the torsional angle ϕ by steps of 10° and optimizing all other internal coordinates. For the potential energy scans, the Becke3LYP functionals[33,34] with the 6-311++G(d,p) basis set were used.

III. Results and Spectroscopic Assignments

According to the DFT calculations, (*E*)-PVA is planar in the ground electronic state. As a result, its 48 normal modes factorize into 33 in-plane modes with a′ symmetry (ν_1−ν_{33}) and 15 out-of-plane modes with a″ symmetry (ν_{34}−ν_{48}). According to the electric dipole selection rules, all in-plane vibrational fundamentals (a′ modes) are allowed, whereas in the case of the a″ modes, only overtones and combination bands with an even number of quanta are predicted to possess nonvanishing intensity.[41] In what follows, the Mulliken numbering[42] scheme will be used to label the observed bands; however, when

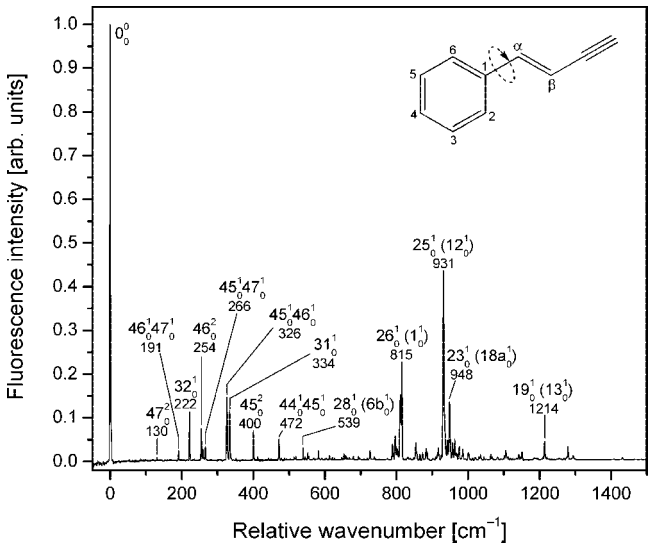

Figure 1. The $S_1 \leftarrow S_0$ fluorescence excitation spectrum of (*E*)-PVA recorded under jet-cooled conditions. The structure and $C_1-C(\alpha)$ torsional motion of (*E*)-PVA are also illustrated.

vibrational modes bear strong resemblances to those in benzene or monosubstituted benzenes, the Wilson scheme[43] will be included in parentheses. Table 1 gives the calculated and experimental vibrational frequencies of both electronic states and approximate descriptions of the motional character of the normal modes in the S_0 state.

As will be shown in more detail in a forthcoming publication,[44] significant mixing of the out-of-plane S_1 normal coordinates with respect to their S_0 counterparts occurs in (*E*)-PVA. Due to this mixing of vibrational coordinates, there is no simple one-to-one correspondence between the normal modes of the S_0 state and those of the S_1 state. Especially noteworthy is the mixing among the four lowest out-of-plane normal modes ν_{45}, ν_{46}, ν_{47}, and ν_{48}. The mixing of these modes will be shown here from the spectra record, whereas a more in-depth analysis of the mixing will be presented elsewhere because it is beyond the scope of this investigation.

A. The Fluorescence Excitation Spectrum of PVA. Figure 1 shows the first 1500 cm^{-1} of the $S_1 \leftarrow S_0$ fluorescence excitation spectrum of the synthesized sample of (*E*)-PVA. The electronic origin was observed at 33 578 cm^{-1}, in agreement with that obtained previously by Robinson et al.[5] from their R2PI spectrum. Table 2 lists the observed positions, relative intensities, and assignments of the main transitions. These assignments are based on an analysis of the SVLF spectra described in Section B. Here, we provide a brief overview of the assigned transitions to highlight the comparison with styrene,[11–14,45] *trans*-β-methylstyrene ($t\beta$MS),[46,47] and a series of alkylbenzenes.[48] The S_1 vibrational frequencies calculated at the CIS level of theory did not reproduce experimentally observed frequencies with an accuracy sufficient to reliably guide the assignment procedure.

Generally, the Franck–Condon (FC) activity in (*E*)-PVA agrees with what is expected for a conjugated, substituted benzene; that is, most of the FC activity lies in ring and substituent-sensitive stretching and bending modes, including prominent FC intensity in modes ν_1, ν_6, ν_{12}, and ν_{13} (in the Wilson numbering scheme).[43] Accordingly, the most intense vibronic band observed in the fluorescence excitation spectrum of PVA, occurring at 931 cm^{-1} above the origin, is assigned to $25_0^1(12_0^1)$, a ring-deformation vibration. The corresponding vibration occurs in styrene[45] and $t\beta$MS[47] at 948 and 927 cm^{-1}, respectively. Other prominent features observed in the excitation spectrum of (*E*)-PVA are the in-plane fundamentals $28_0^1(6b_0^1)$ at 539 cm^{-1}, $26_0^1(1_0^1)$ at 815 cm^{-1}, $23_0^1(18a_0^1)$ at 948 cm^{-1}, and $19_0^1(13_0^1)$ at 1214 cm^{-1}. The band at $0_0^0 + 948$ cm^{-1} was assigned to $23_0^1(18a_0^1)$ on the basis of the relative intensity of this band

TABLE 1: Experimental and Calculated Vibrational Frequencies of Phenylvinylacetylene

		S_0 state		S_1 state	
mode[a]	approximate description[b]	exptl[c]	calcd[d]	exptl[c]	calcd[e]
	A′				
ν_1	≡C−H stretch		3476		3607
ν_2 (2)	ring CH stretch		3192		3379
ν_3	ring CH stretch		3185		3355
ν_4	ring CH stretch		3176		3351
ν_5	ring CH stretch		3167		3342
ν_6	ring CH stretch		3160		3336
ν_7	vinyl CH asym stretch		3153		3329
ν_8	vinyl CH sym stretch		3142		3323
ν_9	C≡C stretch		2189		2153
ν_{10}	C=C stretch		1664		1771
ν_{11} (8a)	ring C−C stretch		1638		1685
ν_{12} (8b)	ring C−C stretch		1612		1644
ν_{13} (19a)	ring C−C stretch	1521	1526		1588
ν_{14} (19b)	ring C−C stretch	1477	1479	1432	1550
ν_{15} (3)	aryl β CH	1372	1364		1449
ν_{16} (15)	ring C−C stretch	1349	1350		1443
ν_{17}	β vinyl C−H	1315	1329		1422
ν_{18}	ring C−C stretch	1287	1294	1279	1326
ν_{19} (13)	C(1)−C(α) stretch	1218	1232	1214	1305
ν_{20} (9a)	aryl β CH	1194	1205		1264
ν_{21} (15′)	aryl β CH		1183	963	1237
ν_{22} (18b)	aryl β CH + ring C−C stretch		1105	942	1175
ν_{23} (18a)	aryl β CH + ring C−C stretch	1048	1051	948	1112
ν_{24}	X sens (C−C stretch)		1031		1071
ν_{25} (12)	ring deform	1011	1014	931	1051
ν_{26} (1)	X sens ring breath	851	858	815	879
ν_{27}	β C≡C−H		688		788
ν_{28} (6b)	X−sens (αC−C−C)	624	636	539	661
ν_{29} (6b)	αC−C−C		632		641
ν_{30}	X−sens (βC−C≡C)	479	493		539
ν_{31}	X sens (αC−C−C)	373	378	334	401
ν_{32}	X−sens (β−CH=CH−C≡)	231	237	222	251
ν_{33}	X−sens (βC−CH=CH−)	105	106	104	117
	A″				
ν_{34} (5)	vinyl + aryl γCH		997		1085
ν_{35}	vinyl + aryl γCH		985		1075
ν_{36} (17a)	aryl γCH		976		969
ν_{37}	vinyl + aryl γCH		927		928
ν_{38}	vinyl + aryl γCH		872		844
ν_{39} (10a)	aryl γCH		846		811
ν_{40} (11)	aryl γCH		766		774
ν_{41} (4)	aryl γCH		698		679
ν_{42}	γC≡C−H		629		650
ν_{43} (16b)	X-sens ring puckering		537		495
ν_{44} (16a)	X-sens ring deform	405	423	275	438
ν_{45} (16a)	ring deform	398	406	201	403
ν_{46}	X-sens (γ C−C=C)	238	248	127	230
ν_{47}	C(1)−C(α) bend	88	90	67	118
ν_{48}	C(1)−C(α) torsion	43	52	348	56

[a] Numbering according to Mulliken.[42] The Wilson scheme[43] is included in parentheses. [b] α, in plane ring angle bend; β, in plane bend; γ, out of plane bend; X-sens, a vibration sensitive to the substituent. Due to the excessive mixing and geometry changes upon excitation, the description should be associated with only the motional character of the normal coordinates in the S_0 state, and not with those in the S_1 state. [c] Experimental frequency, measured from the origin. [d] Ground state frequency calculated with B3LYP/6-311++G(d,p) without scaling. [e] Excited state frequency calculated with CIS /6-311++G(d,p) without scaling.

TABLE 2: Assignments of the LIF Excitation Spectrum of (*E*)-PVA[a]

$\Delta\nu$/cm^{-1}	relative intensity	assignment	$\Delta\nu$/cm^{-1}	relative intensity	assignment
−21[b]		47_1^1	672	0.6	?
0	100	0_0^0	679	1.2	$32_0^1 45_0^1 46_0^1 47_0^2$
24[b]		$47_0^1 48_1^0$	694	1.2	$30_0^1 32_0^1$
84[b]		$46_0^1 48_1^0$	697	0.7	48_0^2
104	0.6	33_0^1	710	0.6	?
130	0.8	47_0^2	718	0.8	?
158[b]		$45_0^1 48_1^0$	724	0.8	$30_0^1 46_0^2$
191	2.5	$46_0^1 47_0^1$	727	2.5	$45_0^3 46_0^1$
222	11	32_0^1	738	1.0	$30_0^1 45_0^1 47_0^1$
232[b]		$44_0^1 48_1^0$	740	0.7	?
254	7.6	46_0^2	752	0.5	$32_0^1 45_0^2 47_0^2$
260	2.8	0_0^0-(*Z*)-PVA	774	0.7	?
266	3.4	$45_0^1 47_0^1$	788	4.0	Fermi resonance
326	15	$45_0^1 46_0^1$, $32_0^1 33_0^1$	791	2.0	Fermi resonance
334	12	31_0^1	797	5.8	Fermi resonance
351	0.7	T_0^2-(*Z*)-PVA	802	2.9	Fermi resonance
400	7.0	$44_0^1 46_0^1$, 45_0^2	805	2.4	Fermi resonance
412	1.1	$47_0^1 48_0^1$, $32_0^1 46_0^1 47_0^1$	810	15	Fermi resonance
442	0.7	32_0^2	815	23	26_0^1
449	0.6	$46_0^3 47_0^1$	831	1.1	$28_0^1 46_0^1 47_0^1$
462	0.5	$31_0^1 47_0^2$	854	4.3	?
472	5.0	30_0^1, $44_0^1 45_0^1$, $46_0^1 48_0^1$	865	1.6	$28_0^1 45_0^1 46_0^1$
478	0.8	$32_0^1 46_0^2$	874	2.1	$28_0^1 31_0^1$, $30_0^1 45_0^2$
480	0.8	?	882	3.1	?
493	0.6	?	886	2.3	$31_0^1 44_0^2$
504	0.7	$31_0^1 45_0^2$	917	3.0	$26_0^1 33_0^1$
514	1.1	46_0^4	931	44	25_0^1
519	1.1	$45_0^1 46_0^2 47_0^1$	943	5.0	22_0^1
539	3.0	28_0^1	948	14	23_0^1, $26_0^1 47_0^2$
545	1.1	?	957	4.0	?
553	2.1	$45_0^1 48_0^1$, 44_0^2	963	5.0	21_0^1
555	1.2	$31_0^1 32_0^1$	976	3.0	?
569	0.8	?	986	2.9	?
576	0.7	$30_0^1 33_0^1$	1001	2.1	810 + 191
582	2.5	$45_0^1 46_0^2$	1035	1.6	$25_0^1 33_0^1$
585	0.7	$45_0^1 46_0^1 47_0^4$	1045	1.1	?
591	0.7	$45_0^2 46_0^1 47_0^1$	1064	1.6	$25_0^1 47_0^2$
593	0.6	$45_0^2 46_0^1 47_0^1$	1068	1.1	$21_0^1 33_0^1$
602	0.7	$30_0^1 47_0^2$	1083	1.0	?
604	0.8	$32_0^2 45_0^2 47_0^2$	1102	1.4	?
613	1.4	?	1106	2.5	?
621	0.8	$32_0^1 45_0^2$	1142	1.6	810 + 334
627	0.8	$45_0^1 46_0^3$	1151	2.2	$25_0^1 32_0^1$, $21_0^1 46_0^1 47_0^1$
647	0.9	?	1214	4.5	19_0^1
653	1.8	$45_0^2 46_0^2$	1279	3.5	18_0^1
658	1.4	$33_0^1 44_0^2$	1294	1.4	?
660	1.0	$31_0^1 45_0^1 46_0^1$	1432	0.9	?
664	0.8	$30_0^1 46_0^1 47_0^1$	1721	0.6	?
668	0.9	$28_0^1 47_0^2$, 31_0^2			

[a] The intensity of each band is relative to the 0_0^0 band origin. [b] Hot bands are not observed in the LIF spectrum under normal jet conditions and are thus excluded in the listing of intensities relative to the 0_0^0 band origin intensity.

with respect to the 12_0^1 band, which compares well with the corresponding relative intensities in the excitation spectra of *tβ*MS[47] and styrene.[45]

The region in which the fundamental of the benzene-mode ν_1 is expected (740−840 cm^{-1}) shows considerable congestion, most likely due to the occurrence of extensive anharmonic mixing between bright and dark states. The SVLF spectra (Section B) lead to an unambiguous assignment of the 815 cm^{-1} transition to $26_0^1(1_0^1)$. This assignment implies a significant spectral shift of mode ν_1 to higher frequency when compared to the observed frequencies of this mode in styrene (746 cm^{-1}) and *tβ*MS (795 cm^{-1}). This increase in frequency can be rationalized by the tendency of mode ν_1 to change its motional character due to a substantial mixing with other modes upon an increase of the substituent chain length.[11,48] The band at 0_0^0 + 1214 cm^{-1} was assigned to $19_0^1(13_0^1)$, in good agreement with the corresponding vibrations occurring in styrene and *tβ*MS at 1209 and 1210 cm^{-1}, respectively. Other weak features in the high-energy region of the fluorescence excitation spectrum become more difficult to assign on account of sizable spectral congestion, most likely due to Fermi resonances with other fundamental and combination bands.

In the low-energy region of the excitation spectrum, the bands at 0_0^0 + 104, 0_0^0 + 222, and 0_0^0 + 334 cm^{-1} are unambiguously assigned to 33_0^1, 32_0^1, and 31_0^1 on the basis of their corresponding SVLF spectra (Section B).

Other transitions in the low-energy region of the excitation spectrum are assigned to even overtones and combinations of out-of-plane vibrational modes ν_{44}−ν_{48}. The assignment of these transitions is complicated by extensive Duschinsky mixing (Section III B.3 and B.4) and the fact that the fundamentals of these out-of-plane vibrations are not allowed. In these cases,

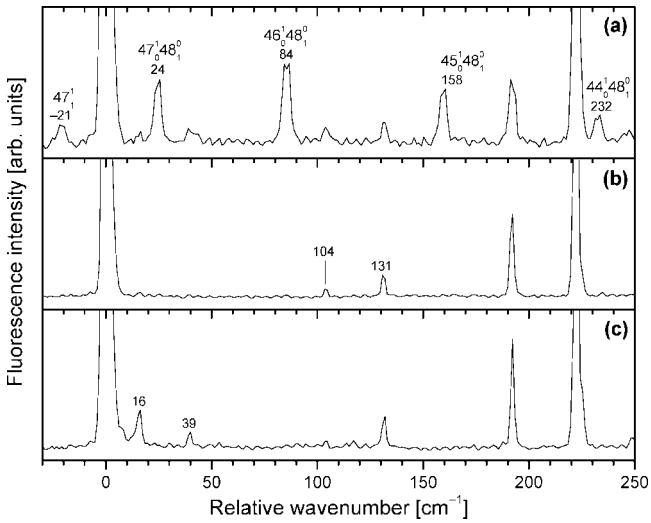

Figure 2. Fluorescence excitation spectra in the region near the $S_1 \leftarrow S_0$ origin of (*E*)-PVA recorded as a function of helium backing pressure: (a) 1 bar, (b) 2.8 bar, and (c) 5.5 bar.

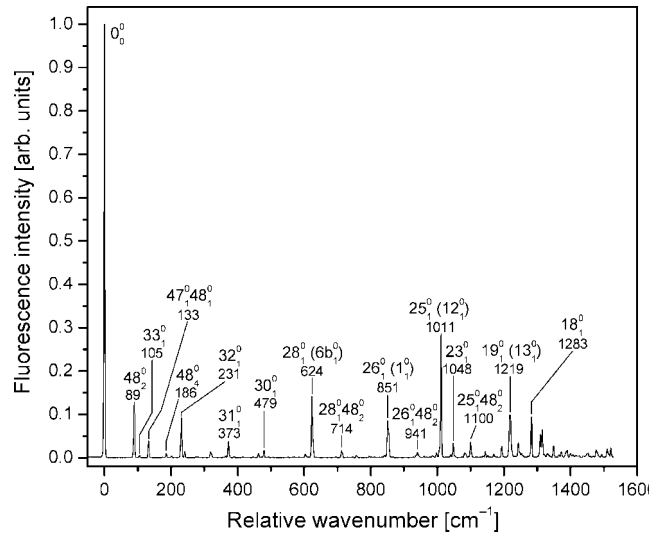

Figure 3. The single vibronic level fluorescence spectrum of (*E*)-PVA with excitation of the electronic origin of the S_1 state.

the identification and assignment of hot bands considerably facilitates the assignment of both S_0 and S_1 normal modes. The important role of hot bands in the assignment process arises because they carry direct information about frequency differences between fundamentals in the S_0 state and the corresponding or even different fundamentals in the S_1 state. In the case of (*E*)-PVA, the assignment of a pair of transitions, consisting of a "hot" and a "cold" transition, containing the fundamentals of ν_{47} in both the S_0 and S_1 states was pivotal to the deduction of the harmonic frequencies of normal modes ν_{44}, ν_{45}, ν_{46}, ν_{47}, and ν_{48} in both the ground and excited electronic states.

To that end, we recorded a series of fluorescence excitation spectra as a function of nozzle backing pressure to identify transitions in the origin region assignable to hot bands (Figure 2). Stagnation pressures of 2.8 bar He yielded a minimum number of bands; that is, the vibronically least congested excitation spectrum (Figure 2b). The appearance of additional bands at $0_0^0 + 16$ and $0_0^0 + 39$ cm^{-1} when the stagnation pressure was raised to 5.5 bar He (Figure 2c) indicated the formation of PVA···He van der Waals complexes under those conditions. On the other hand, stagnation pressures of less than 2.0 bar were not sufficient to completely cool the S_0 population to the vibrationless ground state, leading to the appearance of hot bands in the excitation spectrum at $0_0^0 - 21$, $0_0^0 + 24$, $0_0^0 + 84$, $0_0^0 + 158$, and $0_0^0 + 232$ cm^{-1} (Figure 2a). Additionally, as a result of these stagnation pressure studies, the bands at $0_0^0 + 104$ and $0_0^0 + 130$ cm^{-1} were confirmed to be bare-molecule bands originating in the vibrationless ground state.

B. Single Vibronic Level Fluorescence Spectra of (*E*)-PVA. SVLF spectra were obtained for most strong cold bands and several hot bands appearing in the fluorescence excitation spectrum between −21 and +1279 cm^{-1} of the S_0-S_1 origin of (*E*)-PVA.

1. The 0⁰ SVLF Spectrum. The $S_1 \leftarrow S_0$ origin is the most intense band in the fluorescence excitation spectrum (Figure 1). The SVLF spectrum of this 0_0^0 band is shown in Figure 3. The observed band positions, relative intensities, and assignments are given in Table 3. Computed harmonic frequencies on the B3LYP/6-311++G(d,p) level of theory served as a guide for vibrational assignments in the S_0 state. In line with the calculated frequency values, the lowest frequency band at 89 cm^{-1} was assigned to 48_2^0, the first overtone of the C(1)−C(α) torsional motion. Moreover, accounting qualitatively for the observed intensity pattern, the band at 186 cm^{-1} was assigned to 48_4^0, thus assuming a slightly negative anharmonicity in the torsional coordinate.

Other prominent features observed in the 0^0 SVLF spectrum include the in-plane fundamentals, 32_1^0, 31_1^0, $28_1^0(6b_1^0)$, $26_1^0(1_1^0)$, and $25_1^0(12_1^0)$ (see Figure 3), whose experimentally observed frequencies are in good agreement with the calculated unscaled harmonic frequencies (see Table 1) and the corresponding values of close analogs in related molecules, such as styrene, *tβ*MS, and the alkylbenzenes (Table 4). [11,48] The Wilson notation[43] for benzene-like vibrations is, therefore, also included in Figure 3.

On the basis of the set of computed frequency values, most features in the low-wavenumber region could be assigned to fundamental and combination transitions, gaining confirmation from the analysis of SVLF spectra of other low-lying vibronic transitions, which is taken up in Section B.4.

2. Excitation of In-Plane Normal Modes. Due to the obvious presence of a false origin and their sparse vibrational structure, the SVLF spectra with excitation into the fundamental of an in-plane mode could be readily distinguished from those SVLF spectra that arise from overtone or combination bands of the out-of-plane vibrations. This behavior is illustrated in Figure 4 for the bands at $0_0^0 + 104$, 222, 334, and 539 cm^{-1}, which were assigned to the transitions 33_0^1, 32_0^1, 31_0^1, and 28_0^1, respectively, on the basis of the harmonic frequencies calculated on the B3LYP/6-311++G(d,p) level of theory. The false origins (33_1^1, 32_1^1, 31_1^1, and 28_1^1, respectively) of these SVLF spectra dominate in intensity, appearing at 106, 231, 373, and 624 cm^{-1}, respectively. The band at $0_0^0 + 539$ cm^{-1} in the fluorescence excitation spectrum was assigned to the transition 28_0^1, instead of 29_0^1, due to the occurrence of the false origin 28_1^1 in its SVLF spectrum at 624 cm^{-1}. This assignment was based on the similarity in frequency and form to the S_0 benzene-type vibration $6b_1{}^0$ in styrene (621 cm^{-1}) and *tβ*MS (621 cm^{-1}). Prominent transitions in the 33^1 SVLF spectrum are included in Table 5; the corresponding assignments for the other in-plane bands are included in the Supporting Information.

Figure 5a−d shows the SVLF spectra of the bands at $0_0^0 +$ 810 cm^{-1}, 815 cm^{-1}, 931 cm−1, and 948 cm^{-1}, respectively. Due to obvious anharmonic mixing in the fluorescence excitation spectrum around 800 cm^{-1} (see Figure 1), the SVLF spectra in

TABLE 3: Assignments of the SVLF Spectrum of (*E*)-PVA with Excitation of the S_1 Origin Band[a]

$\Delta\nu$/cm^{-1}	relative intensity	assignment	$\Delta\nu$/cm^{-1}	relative intensity	assignment
0	100	0_0^0	795	0.3	45_2^0
89	13	48_2^0	841	0.6	$30_1^0 47_2^0 48_4^0$
105	0.6	33_1^0	851	8.7	26_1^0
133	3.8	$47_1^0 48_1^0$	941	1.3	$26_1^0 48_2^0$
175	0.2	47_2^0	960	0.4	$26_1^0 33_1^0$
186	1.0	48_4^0	985	0.5	$26_1^0 47_1^0 48_1^0$
202	0.3	$33_1^0 48_2^0$, 33_2^0	997	1.1	$28_1^0 31_1^0$
231	9.3	$47_1^0 48_3^0$, 32_1^0	1011	29	25_1^0
241	1.4	$33_1^0 47_1^0 48_1^0$	1039	0.7	$26_1^0 48_4^0$
275	0.2	$33_1^0 47_2^0$	1048	3.3	23_1^0, 28_2^0
280	0.2	$46_1^0 48_1^0$	1084	1.1	$26_1^0 32_1^0$
319	1.3	$46_1^0 47_1^0$, $32_1^0 48_2^0$	1100	3.7	$25_1^0 48_2^0$
358	0.4	$47_2^0 48_4^0$, $32_1^0 47_1^0 48_1^0$	1144	1.4	$25_1^0 47_1^0 48_1^0$
373	3.7	$46_1^0 48_3^0$, 31_1^0	1168	0.9	?
389	0.6	$33_1^0 46_1^0 48_1^0$	1194	2.6	20_1^0
417	0.3	$46_1^0 47_1^0 48_2^0$	1219	0.9	19_1^0
447	0.9	$45_1^0 48_1^0$	1243	3.6	$25_1^0 32_1^0$
457	0.4	$46_1^0 47_2^0 48_1^0$, $31_1^0 48_2^0$, 32_2^0	1283	9.5	18_1^0
480	1.7	30_1^0, 46_2^0	1309	5.5	$19_1^0 48_2^0$
493	0.2	$45_1^0 47_1^0$	1315	6.5	17_1^0
569	0.2	$46_2^0 48_2^0$, $31_1^0 33_1^0 48_2^0$, $30_1^0 48_2^0$	1349	2.7	16_1^0
604	0.9	$31_1^0 32_1^0$	1372	1.4	?
624	14	28_1^0	1388	1.8	41_1^0, 15_1^0
694	0.2	32_3^0	1451	1.0	$19_1^0 32_1^0$
714	1.7	$28_1^0 48_2^0$	1477	1.8	$26_1^0 28_1^0$, $15_1^0 48_2^0$
746	0.2	31_2^0	1511	1.9	$18_1^0 32_1^0$
756	0.6	$46_3^0 48_1^0$, $28_1^0 47_1^0 48_1^0$	1521	2.4	?

[a] The intensity of each band is relative to the 0_0^0 band origin.

TABLE 4: Comparison of Vibrational Frequencies of Benzene-Type Modes

	ν_{6b}		ν_1		ν_{12}		ν_{18a}		ν_{13}	
molecule	S_0	S_1	S_0	S_1	S_0	S_1	S_0	S_1	S_0	S_1
styrene[a]	624	528	776	746	999	948	1011	959	1204	1209
trans-β-methylstyrene[b]	621	537	821	795	1003	927	1035	959	1208	1210
phenylvinylacetylene[c]	623	539	851	815	1013	931	1048	948	1218	1214
alkylbenzene[d]		526 ± 4		748 ± 18		932 ± 2		966 ± 6		

[a] See ref 12. [b] See ref 47. [c] This work. [d] See ref 48.

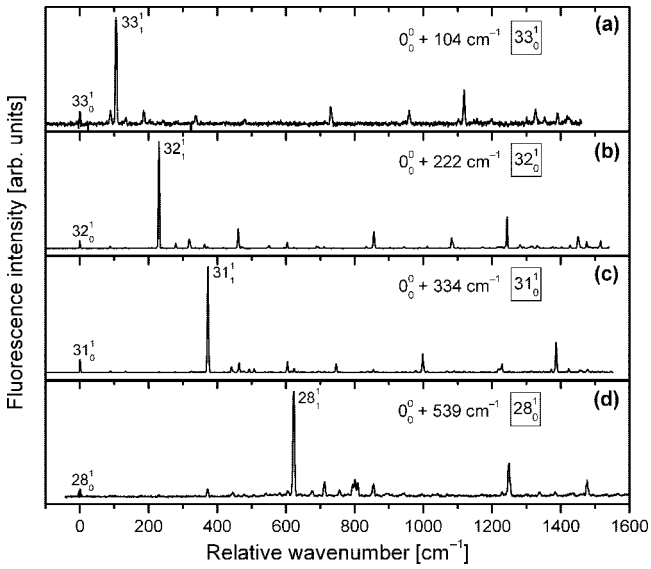

Figure 4. SVLF spectra with excitation of bands involving in-plane motions: (a) 33_0^1, (b) 32_0^1, (c) 31_0^1, and (d) 28_0^1.

this region were difficult to assign. The band at $0_0^0 + 815$ cm^{-1} was tentatively assigned to $26_0^1(1_0^1)$ on the basis of the comparison between the frequency of the most prominent transition (851 cm^{-1}) and the frequency of mode ν_{26} (858 cm^{-1}) calculated at the B3LYP/6-311++G(d,p) level of theory. From an analogous comparison with the calculated frequency of mode ν_{25} (1014 cm^{-1}), the prominent band at 1011 cm^{-1} was assigned to $25_1^0 26_0^1$.

The band at $0_0^0 + 931$ cm^{-1} has been assigned to 25_0^1, even though 25_1^1 at 1011 cm^{-1} is obviously not the most prominent transition in the SVLF spectrum. Several intense bands at 89, 231, and 851 cm^{-1} were assigned to $25_0^1 48_2^0$, $25_0^1 32_1^0$, and $25_0^1 26_1^0$, respectively, on the basis of the assignments of this and the previous section. It should be noted, however, that except for a few prominent bands, most transitions in these SVLF spectra could not be assigned.

SVLF spectra from the levels 726, 788, 1214, and 1279 cm^{-1} above the S_1 origin are included in the Supporting Information, as are tabulated assignments for all recorded SVLF spectra with excitation into the fundamentals of in-plane modes. Characteristic of most SVLF spectra given in Figure 5 is the broad background, upon which sharp transitions are superimposed. This broadening signals the onset of intramolecular vibrational redistribution (IVR) and dominates the spectra at $0_0^0 + 1214$ and $0_0^0 + 1279$ cm^{-1}.

3. SVLF Spectra of Hot Bands. Figure 6a−e shows the SVLF spectra of the hot bands at $0_0^0 - 21$ and $0_0^0 + 24$, 84, 158, and 232 cm^{-1} in the fluorescence excitation spectrum (see Figure 2a). Assignments of prominent bands involving the low-frequency, out-of-plane modes are given in the figure. When

TABLE 5: Representative Assignments of a Hot-Band, an In-Plane Mode Fundamental, and an Out-of-Plane Mode Overtone SVLF Spectrum[a]

47_1^1		33_0^1		47_0^2	
$\Delta\nu$/ cm^{-1}	assignment	$\Delta\nu$/cm^{-1}	assignment	$\Delta\nu$/cm^{-1}	assignment
−45	$47_0^1 48_1^0$	0	33_0^1	0	47_0^2
0	47_1^1	90	$33_0^1 48_2^0$	89	$47_0^2 48_2^0$
50	$47_0^1 48_3^0$	106	33_1^1	104	$33_0^1 47_0^2$
63	$33_1^1 47_1^1 48_0^1$	134	$33_0^1 47_1^0 48_1^0$	132	$47_1^2 48_1^0$
89	$47_1^1 48_2^0$	186	$33_0^1 48_4^0$	153	?
136	$47_2^1 48_1^0$	338	$33_1^1 32_1^0$	175	47_2^2
151	$46_1^0 47_0^1$	480	$33_0^1 31_1^0$, $31_1^0 33_1^1$	201	
231	$47_2^1 48_3^0$, $32_1^0 47_1^1$	713	$28_1^0 33_0^1 48_2^0$		$33_1^0 47_0^2 48_2^0$
280	$46_1^0 47_1^1 48_1^0$	731	$28_1^0 33_1^1$	211	?
374	$46_1^0 47_1^1 48_3^0$	959	$26_1^0 33_1^1$	231	$47_1^2 48_3^0$
	$31_1^0 47_1^1$	1101	$25_1^0 33_0^1 48_2^0$	241	$33_1^0 47_1^2 48_1^0$
480	$46_2^0 47_1^1$, $30_1^0 47_1^1$	1119	$25_1^0 33_1^1$	278	$46_1^0 47_0^2 48_1^0$
580	$28_0^1 47_0^1 48_1^0$	1147	$25_1^0 33_0^1 47_1^0 48_1^0$	314	$47_3^2 48_1^0$
604	$31_1^0 32_1^0 47_1^1$	1156	?	325	$46_1^0 47_1^2$
625	$28_1^0 47_1^1$	1199	$25_1^0 33_0^1 48_4^0$	390	$33_1^0 46_1^0 47_0^2 48_1^0$
689	$28_1^0 33_1^0 47_0^1 48_1^0$	1301	$19_1^0 33_0^1 48_2^0$	407	$33_1^0 47_2^2 48_1^0$
760	$45_2^0 47_0^1 48_1^0$	1326	$19_1^0 33_1^1$	461	$46_1^0 47_2^2 48_1^0$
796	$45_2^0 47_1^1$	1352	$19_1^0 33_0^1 47_1^0 48_1^0$	549	$31_1^0 47_2^2$
807	$26_1^0 47_0^1 48_1^0$	1391	$18_1^0 33_1^1$	758	$46_3^0 47_0^2 48_1^0$
853	$26_1^0 47_1^1$	1421	$17_1^0 33_1^1$		$28_1^0 47_1^2 48_1^0$
967	$25_1^0 47_0^1 48_1^0$			800	$46_3^0 47_1^2$, $28_1^0 47_2^2$
1013	$25_1^0 47_1^1$			941	$26_1^0 47_0^2 48_2^0$
1049	$23_1^0 47_1^1$			986	$26_1^0 47_1^2 48_1^0$
1174	$19_1^0 47_0^1 48_1^0$			1029	$26_1^0 47_2^2$
1220	$19_1^0 47_1^1$			1101	$25_1^0 47_0^2 48_2^0$
1284	$18_1^0 47_1^1$			1145	$25_1^0 47_1^2 48_1^0$
1315	$17_1^0 47_1^1$			1188	$25_1^0 47_2^2$
				1215	$25_1^0 33_1^0 47_0^2 48_2^0$
				1224	$23_1^0 47_2^2$
				1328	$23_1^0 46_1^0 47_0^2 48_1^0$
				1352	$19_1^0 47_1^2 48_1^0$
				1396	$19_1^0 47_2^2$
				1420	$17_1^0 33_1^0 47_0^2$
				1460	$18_1^0 47_2^2$

[a] The complete set of assignments can be found in the Supporting Information.

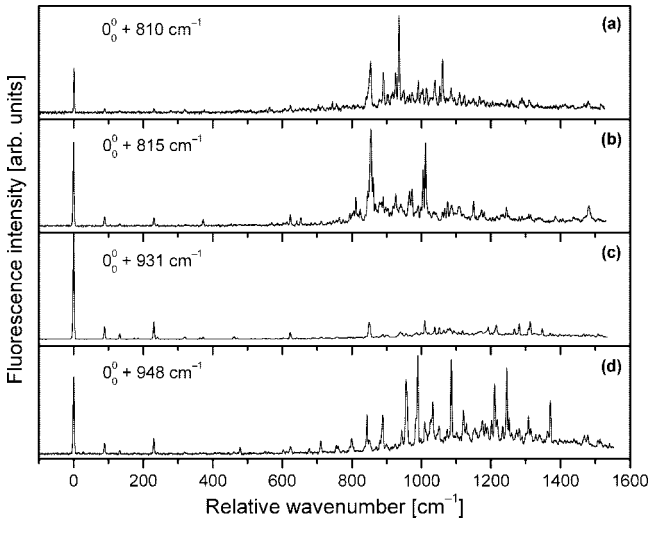

Figure 5. SVLF spectra with excitation of selected transitions (a) 810, (b) 815, (c) 931, and (d) 948 cm^{-1} above the S_1 origin of (*E*)-PVA.

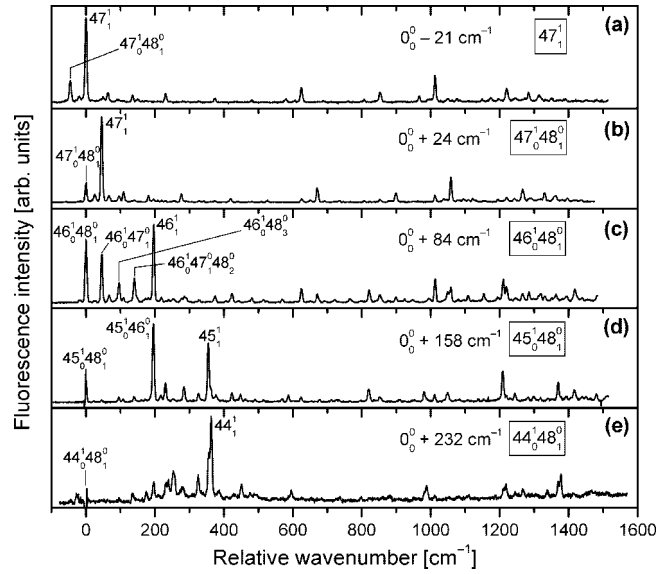

Figure 6. SVLF spectra arising from excitation of hot bands: (a) 47_1^1, (b) $47_0^1 48_1^0$, (c) $46_0^1 48_1^0$, (d) $45_0^1 48_1^0$, and (e) $44_0^1 48_1^0$.

combined with the wavenumber positions of the hot bands in the fluorescence excitation spectra, the SVLF spectra in Figure 6 provide unambiguous assignments for the hot bands at −21, +24, +84, +158, and +232 cm^{-1} as 47_1^1, $47_0^1 48_1^0$, $46_0^1 48_1^0$, $45_0^1 48_1^0$, and $44_0^1 48_1^0$, respectively.

The starting point for these assignments is the fact that the SVLF spectra at $0_0^0 - 21$ cm^{-1} and $0_0^0 + 24$ cm^{-1} are identical in absolute frequency, indicating that these two hot bands share the same upper state level, X^1, but arise from different lower levels. The $0_0^0 - 21$ cm^{-1} spectrum has its dominant emission at the resonance frequency, suggesting its assignment as X_1^1, leaving $0_0^0 + 24$ cm^{-1} as $X_0^1 Y_1^0$. Thus, $\tilde{\nu}_X' - \tilde{\nu}_Y'' = +24$ cm^{-1},

while $\tilde{\nu}_X' - \tilde{\nu}_X'' = -21$ cm^{-1}. The difference between these two equations is just the difference in ground-state vibrational frequencies of the two modes: $\tilde{\nu}_X'' - \tilde{\nu}_Y'' = +45$ cm^{-1}, necessitating an assignment of X as mode 47 (higher wavenumber in S_0) and Y as mode 48 (lower wavenumber in S_0).

The established assignments of the $0_0^0 - 21$ cm^{-1} and $0_0^0 + 24$ cm^{-1} hot bands as 47_1^1 and $47_0^1 48_1^0$, respectively, provides a basis for similar arguments leading to assignments of the $0_0^0 +$ 84, 158 and 232 cm^{-1} hot bands to $46_0^1 48_1^0$, $45_0^1 48_1^0$, and $44_0^1 48_1^0$, respectively. In particular, the SVLF spectra show strong 47_1^1, 46_1^1, 45_1^1, and 44_1^1 bands, respectively, thus not only confirming the S_1 assignments for these hot bands, but also allowing for a determination of the vibrational frequencies $\tilde{\nu}_{44}'$, $\tilde{\nu}_{45}'$, $\tilde{\nu}_{46}'$, and $\tilde{\nu}_{47}'$ in the S_1 state. Assignments of prominent transitions in the SVLF spectra of Figure 6c−e are given in the figure. Detailed assignments for the 47_1^1 hot band are included in Table 5; the assignments of the other hot bands are included in the Supporting Information.

Assuming a Boltzmann distribution over the S_0 vibrational levels and assuming, additionally, that the relative intensities of the hot bands are only determined by their fractional populations, a vibrational temperature of $T_{vib} \approx 30-40$ K can be derived for the fluorescence excitation spectrum of Figure 2a.

One of the most interesting aspects of the hot-band SVLF spectra is the strong Duschinsky mixing among the four out-of-plane coordinates Q_{45}, Q_{46}, Q_{47}, and Q_{48} these spectra reveal. The prominent cross-sequence transitions $46_0^1 47_1^0$ and $46_0^1 48_1^0$ in the $46_0^1 48_1^0$ SVLF spectrum (Figure 6c) and $45_0^1 46_1^0$ and $45_0^1 48_1^0$ in the $45_0^1 48_1^0$ SVLF spectrum (Figure 6d) provide clear evidence for strong Duschinsky mixing among all four coordinates. This four-coordinate Duschinsky mixing has turned out to be amenable to quantitative analyis. The results of these calculations, however, are beyond the scope of this work and will be presented in a forthcoming publication.[44]

4. Cold Bands Involving Out-of-Plane Modes. The vibrational frequencies just established for $\nu_{44}-\nu_{48}$ in both S_0 and S_1 provide a strong basis for assignment of several cold vibronic bands in the excitation spectrum of Figure 1 to even overtones and combination bands involving these modes ($X_0^n Y_0^m$, $n + m = 2$). Thus, the prominent bands 130, 254, and 400 cm^{-1} above the S_1 origin can be assigned to the even overtones 47_0^2, 46_0^2, and 45_0^2, respectively. Similarly, assignments for the combination bands $46_0^1 47_0^1$, $45_0^1 47_0^1$, $45_0^1 46_0^1$, and $45_0^1 44_0^1$ to bands 191, 266, 326, and 472 cm^{-1} above the S_1 origin (Figure 1) immediately follow.

We have not been able to make a firm assignment for the 48_0^2 transition or any combination band involving mode ν_{48} in the excitation spectrum. On the basis of a quantitative Duschinsky analysis,[44] we derived a frequency range $\tilde{\nu}_{48} = 270-350$ cm^{-1}, within which the exact value of mode ν_{48} in the S_1 state most likely lies, and argue for its weak intensity in the excitation spectrum. The precise frequency of ν_{48} in S_1 does not affect the assignment of the fluorescence excitation spectrum given in Table 2. The most likely candidate for 48_0^2 is the weak transition at 697 cm^{-1}. The large increase in frequency predicted for ν_{48} is in keeping with the $\pi-\pi^*$ transition, which adds partial double-bond character to the C(ϕ)−C(α) bond, stiffening the out-of-plane torsion about this bond (ν_{48}). Since PVA retains C_s symmetry upon electronic excitation, there is no shift along the ν_{48} normal coordinate between S_0 and S_1. Therefore, it is not surprising that the 48_0^2 transition shifts to higher frequency in the excitation spectrum and has weak intensity.

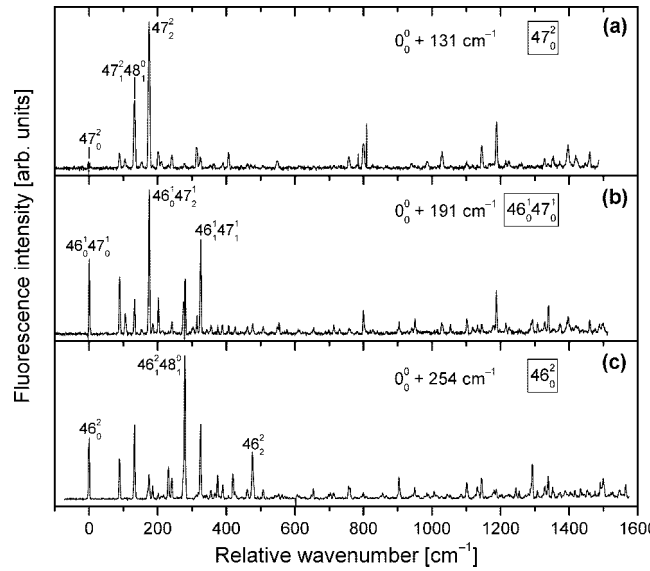

Figure 7. SVLF spectra with excitation of bands involving out-of-plane motions: (a) 47_0^2, (b) $46_0^1 47_0^1$, and (c) 46_0^2.

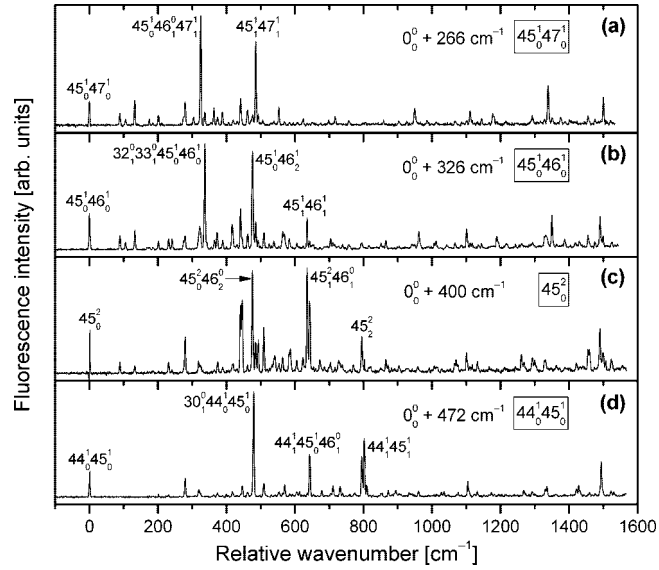

Figure 8. SVLF spectra with excitation of bands involving out-of-plane motions: (a) $45_0^1 47_0^1$, (b) $45_0^1 46_0^1$, (c) 45_0^2, and (d) $44_0^1 45_0^1$.

The assignments for the 47_0^2, $46_0^1 47_0^1$, and 46_0^2 transitions are confirmed by the SVLF spectra of Figure 7a−c, respectively. Not surprisingly, these spectra show large intensity in cross sequence bands involving other members of the $n + m = 2$ series. In fact, in many cases, the cross-sequence bands are more intense than the corresponding main-sequence transitions, consistent with the strong Duschinsky mixing already evident in the hot-band spectra involving these modes. Table 5 lists most of the transitions observed in the 47^2 SVLF spectrum given in Figure 7a, along with their assignments. Once again, the strong cross-sequence bands involve the same modes already identified on the basis of the hot-band spectra.

The SVLF spectra in Figure 8a−d are from additional $X^n Y^m$ levels 266 ($45^1 47^1$), 326 ($45^1 46^1$), 400 (45^2), and 472 cm^{-1} ($44^1 45^1$) above the S_1 origin. In this region, the increasing density of S_1 vibrational levels makes it more likely that the upper levels will experience anharmonic mixing with other levels nearby in energy. In addition, excitation of ν_{45} provides a more complete characterization of Duschinsky mixing involving this mode. Most of the prominent bands in Figure 8 are

sequence or cross-sequence bands involving ν_{45} and ν_{46}, confirming the strong mixing between these two modes in the excited state. Notable exceptions are the strong bands at 337 cm^{-1} in Figure 8b, the unusual number of transitions between 400 and 700 cm^{-1} in Figure 8c, and the transition at 480 cm^{-1} in Figure 8d.

The band at 337 cm^{-1} in Figure 8b can not be assigned to overtones or combination bands involving the out-of-plane modes. The best candidate for this band is a combination of modes ν_{32} (231 cm^{-1}) and ν_{33} (105 cm^{-1}); however, the intensity of this band is roughly 10 times larger than those of the $32_1^0 45_0^1 46_0^1$ and $33_1^0 45_0^1 46_0^1$ transitions. Nonetheless, we tentatively assign the 337 cm^{-1} band to $32_1^0 33_1^0 45_0^1 46_0^1$, on the basis of a likely Fermi resonance between the S_1 levels $32^1 33^1$ and $45^1 46^1$, which would give rise to a local mixing of vibrational wave functions, thus creating the impression of Duschinsky mixing between vibrational coordinates of different symmetry. This explanation requires a weak coupling of less than 1 cm^{-1} between the two vibrational wave functions, because there is no evidence for broadening or splitting of the $0_0^0 + 326$ cm^{-1} band in the excitation spectrum due to the presence of two transitions.

The 45^2 SVLF spectrum of Figure 8c exhibits an intriguing complexity. The most intense band at 636 cm^{-1} was assigned to $45_1^2 46_1^0$, in line with the signficant Duschinsky mixing between normal coordinates Q_{45} and Q_{46} previously encountered in the $45^1 47^1$ SVLF spectrum. Other prominent features at 441, 446, 643, and 795 cm^{-1} were assigned to $45_1^2 48_1^0$, $44_1^0 45_0^2 48_1^0$, $44_1^0 45_0^2 46_1^0$, and 45_2^2, respectively. The assignments involving mode ν_{44} were based on the S_0 harmonic frequency $\tilde{\nu}''_{44} = 423$ cm^{-1} calculated on the B3LYP/6-311++G(d,p) level of theory, which agrees well with the experimentally derived value of 643 $cm^{-1} - \tilde{\nu}''_{46} = 643$ $cm^{-1} - 238$ $cm^{-1} = 405$ cm^{-1}. The reason for the appearance of these bands, however, is best understood as arising from a near-degenerate Darling−Dennison resonance between two weakly coupled vibrational levels, 45^2 and $44^1 46^1$.[49] The possibility of strong Duschinsky mixing between Q_{44} and Q_{45} is a less probable explanation, since the $45^1 47^1$ and the $45^1 46^1$ SVLF spectra do not provide evidence for such mixing.

Finally, the SVLF spectrum of Figure 8d has its most prominent band at 480 cm^{-1}. Taking into account that the 480 cm^{-1} band in the 0^0 SVLF spectrum was previously assigned to 30_1^0, it might seem obvious that the SVLF spectrum of Figure 8(d) originates from the 30^1 level. This SVLF spectrum, however, is not as simple as those given in Figure 4 involving the excitation of in-plane vibrations because there is also clear evidence for numerous, unusually prominent transitions terminating in combination levels of out-of-plane vibrations. Two possibilities exist: First, this spectrum is originating from a mixed upper state involving two near-degenerate levels, 30^1 and $44^1 45^1$. In this case, we would label the 480 cm^{-1} transition as $30_1^0 44_0^1 45_0^1$. Alternatively, as we shall see in the next section, the $0_0^0 + 472$ cm^{-1} band is overlapped with a vibronic transition due to (*Z*)-PVA, which could give rise to the transition at 480 cm^{-1}. Full assignments for the six SVLF spectra in Figure 7b,c and Figure 8a−d can be found in the Supporting Information.

C. Assignment of Transitions Due to (*Z*)-PVA. The one-color R2PI spectrum of PVA in the region of the $S_1 \leftarrow S_0$ electronic transition is given in the upper trace of Figure 9. The R2PI spectrum spans ~1800 cm^{-1} and shows increasing congestion and broadening at higher energies. The intensity patterns are quite different from the fluorescence excitation spectrum (Figure 1) due to saturation of many transitions under the laser power conditions used for the R2PI spectrum. UVHB spectroscopy was employed to determine whether conformational or structural isomers contribute to the R2PI spectrum. The lower trace of Figure 9 shows the UVHB spectrum recorded with the hole-burn laser fixed at the (*E*)-PVA 0_0^0 band. Even though most observed transitions obviously arise from the S_0 zero-point level of (*E*)-PVA, a closer inspection reveals that the band at $0_0^0 + 260$ cm^{-1} (inset) and a smaller band at $0_0^0 + 351$ cm^{-1} are not duplicated in the UVHB spectrum. The more intense band at $0_0^0 + 260$ cm^{-1} is found in both the R2PI spectrum and the fluorescence excitation spectrum (Figure 1) and turned out to be independent of a wide range of expansion conditions and nozzle positions relative to the excitation laser beam. It was, therefore, concluded that the 260 cm^{-1} band is most likely not due to helium complexes or hot bands.

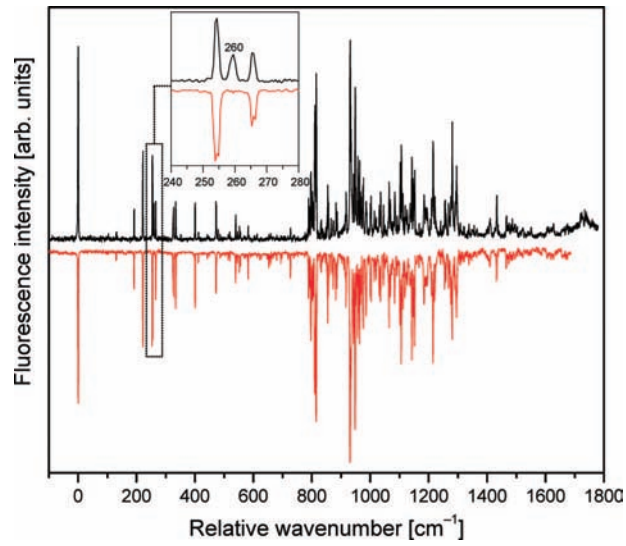

Figure 9. One-color R2PI spectrum (upper trace) and UV−UV hole-burning spectrum (lower trace) with the hole-burn laser fixed at the origin band of (*E*)-PVA. The inset shows an expanded view of the region around 260 cm^{-1} where a transition in the R2PI spectrum does not burn with (*E*)-PVA.

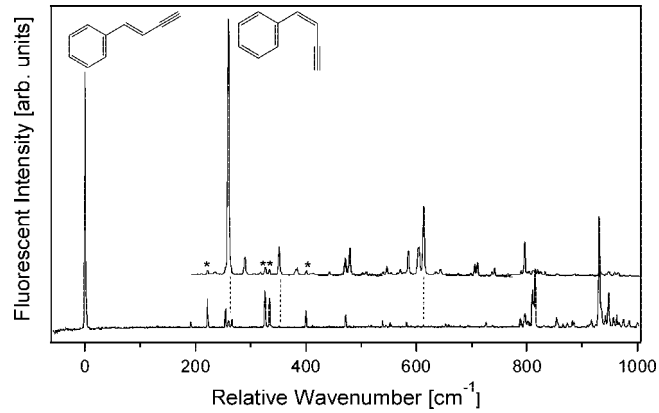

Figure 10. Overlaid LIF spectra of (*E*)-PVA (lower trace) and (*Z*)-PVA (upper trace). Vertical dashed lines are used to indicate signatures of the *Z*-isomer that appear (as an impurity) in the *E*-isomer spectrum. Asterisks indicate transitions dues to the *E*-isomer (as an impurity) in the *Z*-isomer spectrum.

To test the possibility that these transitions are due to (*Z*)-PVA, this isomer was synthesized, and its LIF excitation spectrum was recorded. Figure 10 compares the LIF spectra of the synthesized samples of (*E*)-PVA (lower trace) and (*Z*)-PVA (upper trace). The S_0-S_1 origin of (*Z*)-PVA is 260 cm^{-1} above that of (*E*)-PVA, proving that the unassigned transitions in the

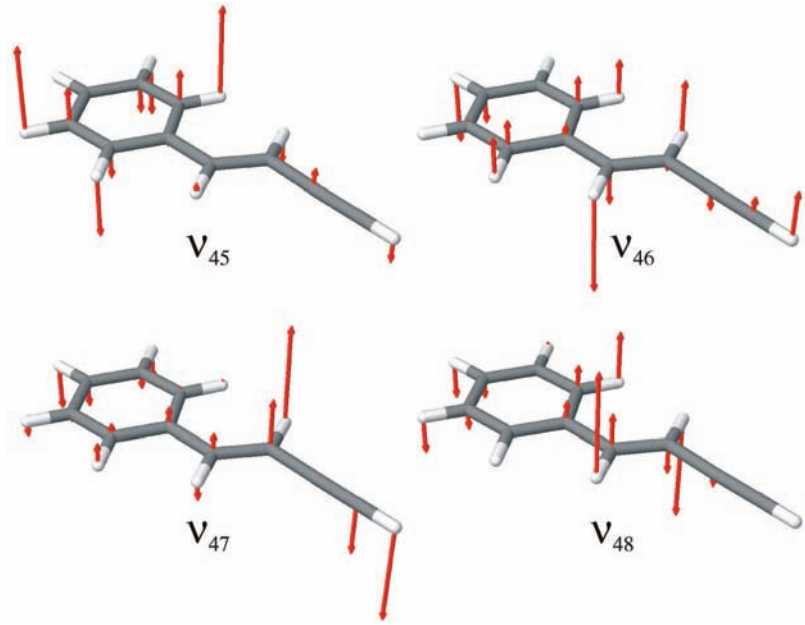

Figure 11. Ground state normal coordinates for modes 45, 46, 47, and 48 calculated on the B3LYP/6-311++G(d,p) level of theory. Mode 48 in the ground state is the phenyl−vinyl torsional mode whose energy levels are used to fit the torsional potential.

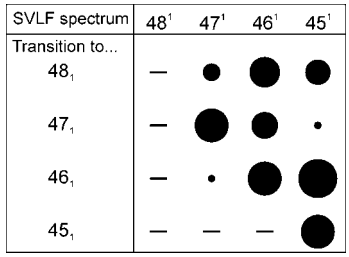

Figure 12. Pictorial representation of the peak intensities of the main-sequence (diagonal circles) and cross-sequence (off-diagonal circles) transitions observed in the 48^1, 47^1, 46^1, and 45^1 SVLF spectra. The circle areas represent the peak intensities of the corresponding transitions. The peak intensities of all main-sequence transitions (diagonal circles) were normalized to unity.

(*E*)-PVA spectrum are due to a minor (*Z*)-PVA impurity in the sample. The corresponding transitions due to (*E*)-PVA are observable as minor impurities in the (*Z*)-PVA spectrum. The spectroscopy of (*Z*)-PVA will be taken up elsewhere.[50]

IV. Analysis and Discussion

The results just presented have led to a near complete vibronic assignment of the excitation spectrum and a series of SVLF spectra of (*E*)-PVA. Much of this structure has involved five low-frequency out-of-plane modes, $\nu_{44}-\nu_{48}$, four of which undergo extensive Duschinsky mixing upon electronic excitation. Figure 11 presents the form of these normal modes in the ground electronic state, as predicted by DFT B3LYP/6-311++G(d,p) calculations. In lieu of a full quantitative analysis, we use the intensities of the strong cross sequence bands in the hot-band spectra to read off which modes are strongly mixed upon electronic excitation, as depicted in Figure 12. It is obvious from this matrix that Duschinsky mixing between these four modes is extensive so that the form of the normal modes in the excited state is a strong admixture of those in the ground state (Figure 11).

Table 1 highlights the large changes in the frequencies of these modes upon electronic excitation, with modes 44−47 lowering their frequency, sometimes by more than a factor of 2. In contrast, mode 48 has its frequency raised significantly, by an amount that is only surmised on the basis of the quantitative Duschinsky analysis described elsewhere.[44] As Figure 11 shows, in the ground state, ν_{48} is the phenyl−vinyl torsion that has a close analog in styrene. The increased double bond character in C(1)−C(α) is responsible for the increased frequency of this mode and reflects in a general way the increased barrier to internal rotation about this bond in S_1 relative to S_0. Since ν_{48} has not been identified with certainty in the S_1 state, we cannot use its progression to deduce the barrier height in the S_1 state. However, the SVLF spectra do enable a hindered rotor analysis in the ground state. It is to this that we now turn.

A. Torsional Potentials of PVA. As in the case of the 0^0 SVLF spectrum of styrene, the 0^0 SVLF spectrum of (*E*)-PVA contains only two overtone transitions of the C(1)−C(α) torsional coordinate (48_2^0 at $0_0^0 - 89$ cm^{-1} and 48_4^0 at $0_0^0 - 186$ cm^{-1}). This allows for the determination of only two torsional frequency spacings in the S_0 state, $\tilde{\nu}(48_{2\leftrightarrow 0})$ and $\tilde{\nu}(48_{4\leftrightarrow 2})$. In the case of styrene, however, the 0^0 SVLF spectrum in combination with the $41_0^1 42_0^1$ SVLF spectrum[12,51] allowed for the determination of S_0 torsional frequency spacings for $v_{42} = 0-5$ and gas-phase Raman spectra[12,52] for the determination of additional levels up to $v_{42} = 17$. In an analogous way, by using assigned transition frequencies from either the $47_1^0 48_0^1$, $46_0^1 48_1^0$, or $45_0^1 48_1^0$ SVLF spectrum, four S_0 torsional frequency spacings $\tilde{\nu}(48_{(n+1)\leftrightarrow n})$ with $n = 0, 1, 2, 3$ can be derived for (*E*)-PVA. This derivation requires the assumption that one of the modes 45−47 is harmonic up to $v'' = 2$. Since this assumption seems better justified for a high-frequency vibration, we assume harmonicity in mode 45 using the $45_0^1 48_1^0$ SVLF spectrum. This leads to 1−0, 2−1, 3−2, and 4−3 S_0 torsional frequency spacings of 42, 47, 48, and 49 cm^{-1}, respectively, exhibiting the same negative anharmonicity found for the analogous torsional mode in styrene (38.1, 48.3, 53.7, 56.5, and 59.0 cm^{-1} $v'' = 1-0$, 2−1, 3−2, 4−3, and 5−4 intervals[12]).

The S_0 torsional potential of (*E*)-PVA was simulated following a previously described fitting procedure[53] using the method of Laane and co-workers.[54] The eigenvalues, E_v, of an internal rotation Hamiltonian,

$$H\Psi_v = \left[-B\frac{\partial^2}{\partial\varphi^2} + V(\varphi)\right]\Psi_v = E_v\Psi_v \quad (1)$$

were matched in an automated fitting procedure to the experimentally derived frequency spacings. For this purpose, an unweighted least-squares sum fit function,

$$F_{\Delta\nu} = \sum_{i=1}^{4}\left[\Delta\nu_i^{\text{calc}} - \Delta\nu_i^{\text{exp}}\right]^2 \quad (2)$$

was minimized using a simplex search algorithm[55] with the goal of finding a set of optimized potential parameters V_n for the truncated Fourier expansion,

$$V(\varphi) = \frac{1}{2}\sum_{n=1}^{4} V_n[1 - \cos(n\varphi)] \quad (3)$$

approximating the periodic torsional potential function of eq 1. Due to the planar symmetry of (*E*)-PVA, the expected 2-fold torsional barrier and, moreover, the limited number of experimental frequency spacings, only V_2 and V_4 were taken into account, where, for $|V_4| < |V_2|/4$, V_2 corresponds to the torsional barrier, and V_4 represents the anharmonicity of the torsional potential. In eq 2, $\Delta\nu_i^{\text{calc}}$ and $\Delta\nu_i^{\text{exp}}$ denote the calculated and experimental frequency spacings, respectively. The internal rotation constant B was assumed to be independent of the torsional angle ϕ (see Figure 1) and was calculated according to

$$B = \frac{h}{8\pi^2 c I_r} \quad (4)$$

using the reduced moment of inertia I_r as defined by Pitzer.[56] An attempt to calculate the effective moment of inertia according to the more accurate procedure for asymmetric internal rotors introduced by Wong, Thom, and Field[57] turned out to be computationally infeasible for a molecule of the size of PVA, and we did not pursue it further. A value of $B = 1.5351$ cm^{-1} was obtained from the S_0 equilibrium geometry calculated on the B3LYP/6-311++G(d,p) level of theory. The best-fit S_0 torsional potential with potential parameter values of $V_2 = 688$ cm^{-1} and $V_4 = -114$ cm^{-1} is displayed in Figure 13. Table 6 gives the comparison between the experimentally observed and simulated spacings and, as a reference, the experimentally observed spacings of the torsional term values in styrene. In an attempt to provide supporting evidence for the significance and accuracy of the simulated torsional potential, we also carried out ab initio and DFT calculations of the torsional potential energy curve at different levels of theory. A comparison between the potential parameters obtained from fits to these potential energy scans and the potential parameters obtained from the simulation is given in Table 7. All methods (except for the HF and MP2 calculations) yield the same overall shape of the potential energy curve as the simulation; that is, they all predict a planar equilibrium geometry and an anharmonically broadened potential well. They differ drastically, however, with respect to the barrier height and the degree of anharmonicity. The potential energy scans yield torsional barriers that are higher in energy than the experimentally derived barrier by a factor 1.6−3.2 and stronger anharmonicities by a factor of 2.8−3.7. As previously observed in the case of 2-phenylindene,[53] the MP2 calculation yields the closest agreement with respect to the barrier height but fails to account for a planar S_0 equilibrium geometry. Moreover, torsional transition state geometries and vibrational frequencies were calculated for the S_0 state. Transition states were located using the synchronous transit-guided quasi-Newton method[58,59] using B3LYP 6-311++G(d,p) for the ground state (using the QST3 keyword). The calculated transition state of the torsion matches that of the torsional potential energy surface, confirming that it is, indeed, a first-order transition state. The calculated transition state was found to be 1685 cm^{-1} above the ground-state zero-point level, in good agreement with the torsional potential energy surface.

A firm resolution of this apparent discrepancy between experiment and theory could take several paths. First, barrier height calculation at higher levels of theory may reduce the barrier still further until it comes in close agreement with experiment. Alternatively, an expanded data set containing

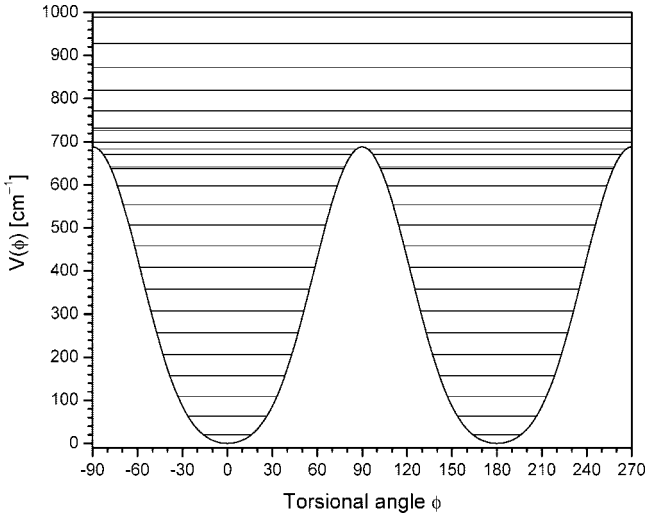

Figure 13. Simulated torsional potential curve of (*E*)-PVA in the S_0 state.

TABLE 6: Torsional Progression in Phenylvinylacetylene and Styrene

phenylvinylacetylene[a]			styrene[b]	
ν_{48}	exptl/cm^{-1}	calcd/cm^{-1}	ν_{42}	exptl/cm^{-1}
1	42[c]	43	1	38.1
2	89[d]	89	2	86.4
3	137[c]	137	3	140.1
4	186[d]	186	4	196.6
			5	255.6

[a] This work. Calculated values from eq 1. [b] See ref 12. [c] The values for $n = 1$ and 3 are derived according to the procedure found in the text (Section IV A). [d] The values for $n = 2$ and 4 are the frequencies found in the LIF spectrum.

TABLE 7: Comparison between the Potential Parameters Obtained from Fits to the ab Initio Calculated Potentials and the Potential Parameters Obtained from the Simulation According to Eq 3 for the S_0 State of PVA

method	V_2/cm^{-1}	V_4/cm^{-1}	E_0/cm^{-1}
HF/6-311++G(d,p)	1095	−297	1097
B3LYP/6-311++G(d,p)	1674	−320	1674
B3PW91/6-311++G(d,p)	1647	−329	1647
MPW1PW91/6-311++G(d,p)	1631	−331	1631
SVWN/6-311++G(d,p)	2150	−391	2150
BLYP/6-311++G(d,p)	1801	−329	1801
MP2/6-31+G(d,p)	846	−496	1009
PVA: simulation	688	−114	688
STY: simulation[a]	1070	−275	1070
STY: B3LYP/6-311++G(d,p)	1365	−274	1365

[a] ref. [23]

higher-energy torsional levels that reach closer to the barrier height could provide a more well-characterized torsional potential. Finally, direct experimental measurement of a slightly asymmetrized isotopomer (which by that virtue would have two conformational isomers) could be undertaken, using stimulated emission pumping-population transfer spectroscopy.[60–63]

B. Structural Isomerization in PVA. The present study has characterized in some detail the vibronic spectroscopy of a key $C_{10}H_8$ structural isomer, (*E*)-PVA. We have also identified the vibronic spectrum of (*Z*)-PVA as an impurity in the spectrum of the *E*-isomer and subsequently verified this fact by recording the fluorescence excitation spectrum of a synthesized sample of the (*Z*)-PVA isomer.

This spectroscopic study provides a necessary foundation for planned studies of the photoisomerization between these two isomers: $E \leftrightarrow Z$. This isomerization is closely analogous to the cis−trans isomerization in stilbene ($C_6H_5-CH=CH-C_6H_5$), a process that has been studied in some detail.[64–71] In the ground state, cis−trans isomerization in stilbene occurs over a very large barrier; however, this barrier drops to ∼1200 cm^{-1} in the S_1 state of the trans isomer,[65,66,72] leading to a surface crossing that returns the molecule with about equal probability to the trans and cis ground-state wells. It is therefore possible in *trans*-stilbene to pump vibronic levels starting from the S_1 origin and extending above the barrier, thereby enabling a determination of the energy-dependent isomerization rate $k_{isom}(E)$ in S_1 simply by measuring the S_1 state lifetime as a function of excitation energy.[72]

In many ways, the R2PI spectrum in (*E*)-PVA is reminiscent of that in *trans*-stilbene, with Franck−Condon activity extending about 1300 cm^{-1} above the S_1 origin. The absence of significant vibronic activity above 1300 cm^{-1} could be the result of small Franck−Condon factors in this region; however, it is more likely that the intensity reduction reflects a decrease in the fluorescence quantum yield as the excited-state lifetime shortens via the onset of a nonradiative process. Furthermore, as in *trans*-stilbene, this spectral reduction occurs right in the region where broadened emission indicates the onset of IVR. This was evident in the spectra in Figure 5 as the broad origin-like emission, which begins to appear about 900 cm^{-1} above the S_1 origin and dominates the spectrum in bands above 1200 cm^{-1} (see SVLF spectra in the Supporting Information).

It seems likely that (*E*)-PVA will utilize a pathway for structural isomerization that is similar to that in *trans*-stilbene. Furthermore, since the ultraviolet spectrum of (*Z*)-PVA is also sharp and in the same wavelength region, PVA presents itself as an ideal case for studying $E \rightarrow Z$ and $Z \rightarrow E$ photoisomerization and to search for mode-specific effects.

Finally, from a structural viewpoint, the *Z*-isomer may play an important role as a key intermediate along the pathway to closure of the second ring to produce naphthalene. As such, it is an ideal isomeric starting point for UV-induced population transfer (UV-PT) studies detecting naphthalene downstream. Zimmerman and co-workers have demonstrated the formation of naphthalene from PVA in flash vacuum pyrolysis[73,74] and explored the cycloisomerization mechanisms in detail.[75,76] All of this suggests that a UV-population transfer experiment involving (*E*)-PVA, (*Z*)-PVA, and naphthalene should be possible.

V. Conclusions

The vibronic structure of the S_0-S_1 transition in jet-cooled PVA was investigated in detail by using fluorescence excitation, UVHB, R2PI, and SVLF spectroscopy. Hot-band SVLF spectra proved particularly helpful in the assignment of transitions involving the low-frequency, out-of-plane normal vibrations ν_{45}, ν_{46}, ν_{47}, and ν_{48}. These spectra provided clear evidence for strong Duschinsky mixing among these four normal coordinates in the S_1 state relative to their S_0 counterparts. The one-dimensional torsional potential in the S_0 state of PVA was simulated using four torsional frequency spacings determined from hot-band SVLF spectra. This potential resembles the S_0 torsional potential of styrene with respect to the barrier height and the degree of anharmonicity, indicating that the extended conjugation in PVA has little effect on the S_0 torsional motion.

We have also recorded the LIF excitation spectrum of (*Z*)-PVA in preparation for its more detailed spectroscopic and photochemical study. Its $S_1 \leftarrow S_0$ 0_0^0 transition was assigned to the band 260 cm^{-1} blue-shifted from the *E*-isomer electronic origin. This finding is particularly interesting from the point of view of the mechanisms for formation of PAHs. In previous flash vacuum pyrolysis studies,[73,74] PVA was found to cycloisomerize thermally into naphthalene. The cycloisomerization of PVA is, thus, of possible relevance to PAH growth processes in sooting flames, discharges, interstellar media, and Titan's atmosphere. The ring closure mechanism, which has been studied in detail for high temperatures,[75,76] requires at low temperatures as a first step the isomerization of (*E*)-PVA into (*Z*)-PVA. In the future, double-resonance experiments could be carried out to determine the energy differences between the two isomers and the barriers to conformational isomerization. Analogous experiments have already been carried out on *m*-ES,[6,7] another $C_{10}H_8$ isomer of naphthalene.

Acknowledgment. The authors gratefully acknowledge support from the NASA Planetary Atmospheres program (NNG06GC57G) for this research. The calculations described in this work were carried out using computing resources provided by Information Technology at Purdue−the Rosen Center for Advanced Computing at Purdue. C.P.L. thanks the Taiwan NSC for financial support through a Taiwan Merit Scholarship (TMS-094-2-B-020) during her postdoctoral research at Purdue University. C.W.M. thanks the Deutsche Akademie der Naturforscher Leopoldina for a postdoctoral scholarship (Grant no. BMBF-LPD 9901/8-159 of the Bundesministerium für Bildung und Forschung). J.J.N. acknowledges the technical and computational advice and expertise provided by William H. James III.

Supporting Information Available: Complete assignments of SVLF spectra. This material is available free of charge via the Internet at http://pubs.acs.org.

Note Added in Proof. We would like to point out that the assignment of the S_0 vibrational level at 186 cm^{-1} to 48_4 was based on frequency spacing evidence (Table 6) only. This assignment allowed for the best agreement between the observed and experimentally derived frequency spacings on one hand (column 2 of Table 6) and the simulated spacings on the other hand (column 3 of Table 6). There is, however, an alternative possibility for the assignment of 48_4 based on intensity evidence only. This alternative is the band at 201 cm^{-1}. This assignment allows for a better agreement between the experimentally observed intensities of this band in different SVLF spectra and those calculated in our Duschinsky fitting procedure. We will address this ambiguity in greater detail in a forthcoming publication.[44]

References and Notes

(1) Frenklach, M. *Phys. Chem. Chem. Phys.* **2002**, *4*, 2028.
(2) Filley, J.; McKinnon, J. T. *Combust. Flame* **2001**, *124*, 721.
(3) Goldaniga, A.; Faravelli, T.; Ranzi, E. *Combust. Flame* **2000**, *122*, 350.
(4) Roesler, J. F.; de Tessan, M. A.; Montagne, X. *Chemosphere* **2001**, *42*, 823.
(5) Robinson, A. G.; Winter, P. R.; Zwier, T. S. *J. Phys. Chem. A* **2002**, *106*, 5789.
(6) Selby, T. M.; Meerts, W. L.; Zwier, T. S. *J. Phys. Chem. A* **2007**, *111*, 3697.
(7) Selby, T. M.; Zwier, T. S. *J. Phys. Chem. A* **2007**, *111*, 3710.
(8) Güthe, F.; Ding, H. B.; Pino, T.; Maier, J. P. *Chem. Phys.* **2001**, *269*, 347.
(9) Yin, H. M.; Heazlewood, B. R.; Stamford, N. P. J.; Nauta, K.; Bacskay, G. B.; Kable, S. H.; Schmidt, T. W. *J. Phys. Chem. A* **2007**, *111*, 3306.
(10) Head-Gordon, M.; Pople, J. A. *J. Phys. Chem.* **1993**, *97*, 1147.
(11) Hollas, J. M.; Khalilipour, E.; Thakur, S. N. *J. Mol. Spectrosc.* **1978**, *73*, 240.
(12) Hollas, J. M.; Ridley, T. *Chem. Phys. Lett.* **1980**, *75*, 94.
(13) Hollas, J. M.; Ridley, T. *J. Mol. Spectrosc.* **1981**, *89*, 232.
(14) Ribblett, J. W.; Borst, D. R.; Pratt, D. W. *J. Chem. Phys.* **1999**, *111*, 8454.
(15) Schaefer, T.; Penner, G. H. *Chem. Phys. Lett.* **1985**, *114*, 526.
(16) Tsuzuki, S.; Tanabe, K.; Osawa, E. *J. Phys. Chem.* **1990**, *94*, 6175.
(17) Hemley, R. J.; Leopold, D. G.; Vaida, V.; Karplus, M. *J. Chem. Phys.* **1985**, *82*, 5379.
(18) Dierksen, M.; Grimme, S. *J. Chem. Phys.* **2004**, *120*, 3544.
(19) Duschinsky, F. *Acta Physicochim. URSS* **1937**, *7*, 551.
(20) Bock, C. W.; Trachtman, M.; George, P. *Chem. Phys.* **1985**, *93*, 431.
(21) Hemley, R. J.; Leopold, D. G.; Vaida, V.; Karplus, M. *J. Chem. Phys.* **1985**, *82*, 5379.
(22) Choi, C. H.; Kertesz, M. *J. Phys. Chem. A* **1997**, *101*, 3823.
(23) Hollas, J. M. *J. Chem. Soc., Faraday Trans.* **1998**, *94*, 1527.
(24) Smith, W. L. *J. Mol. Spectrosc.* **1998**, *187*, 6.
(25) Hollas, J. M.; Musa, H.; Ridley, T.; Turner, P. H.; Weisenberger, K. H.; Fawcett, V. *J. Mol. Spectrosc.* **1982**, *94*, 437.
(26) Prall, M.; Kruger, A.; Schreiner, P. R.; Hopf, H. *Chem.—Eur. J.* **2001**, *7*, 4386.
(27) Selby, T. M.; Clarkson, J. R.; Mitchell, D.; Fitzpatrick, J. A. J.; Lee, H. D.; Pratt, D. W.; Zwier, T. S. *J. Phys. Chem. A* **2005**, *109*, 4484.
(28) Majewski, W.; Meerts, W. L. *J. Mol. Spectrosc.* **1984**, *104*, 271.
(29) Plusquellic, D. F.; Davis, S. R.; Jahanmir, F. *J. Chem. Phys.* **2001**, *115*, 225.
(30) Pillsbury, N. R.; Plusquellic, D. F.; Zwier, T. S. Manuscript in preparation, 2008.
(31) Michel, P.; Gennet, D.; Rassat, A. *Tetrahedron Lett.* **1999**, *40*, 8575.
(32) Frisch, M. J.; Trucks, G. W.; Schlegel, H. B.; Scuseria, G. E.; Robb, M. A.; Cheeseman, J. R.; Montgomery, J. A.; n/a, T. V., Jr.; Kudin, K. N.; Burant, J. C.; Millam, J. M.; Iyengar, S. S.; Tomasi, J.; Barone, V.; Mennucci, B.; Cossi, M.; Scalmani, G.; Rega, N.; Petersson, G. A.; Nakatsuji, H.; Hada, M.; Ehara, M.; Toyota, K.; Fukuda, R.; Hasegawa, J.; Ishida, M.; Nakajima, T.; Honda, Y.; Kitao, O.; Nakai, H.; Klene, M.; Li, X.; Knox, J. E.; Hratchian, H. P.; Cross, J. B.; Bakken, V.; Adamo, C.; Jaramillo, J.; Gomperts, R.; Stratmann, R. E.; Yazyev, O.; Austin, A. J.; Cammi, R.; Pomelli, C.; Ochterski, J. W.; Ayala, P. Y.; Morokuma, K.; Voth, G. A.; Salvador, P.; Dannenberg, J. J.; Zakrzewski, V. G.; Dapprich, S.; Daniels, A. D.; Strain, M. C.; Farkas, O.; Malick, D. K.; Rabuck, A. D.; Raghavachari, K.; Foresman, J. B.; Ortiz, J. V.; Cui, Q.; Baboul, A. G.; Clifford, S.; Cioslowski, J.; Stefanov, B. B.; Liu, G.; Liashenko, A.; Piskorz, P.; Komaromi, I.; Martin, R. L.; Fox, D. J.; Keith, T.; Al-Laham, M. A.; Peng, C. Y.; Nanayakkara, A.; Challacombe, M.; Gill, P. M. W.; Johnson, B.; Chen, W.; Wong, M. W.; Gonzalez, C.; Pople, J. A. *Gaussian 03*; Revision C.02 ed.; Gaussian, Inc.: Wallingford, CT, 2004.
(33) Becke, A. D. *J. Chem. Phys.* **1993**, *98*, 5648.
(34) Lee, C. T.; Yang, W. T.; Parr, R. G. *Phys. Rev., B* **1988**, *37*, 785.
(35) Frisch, M. J.; Pople, J. A.; Binkley, J. S. *J. Chem. Phys.* **1984**, *80*, 3265.
(36) Krishnan, R.; Binkley, J. S.; Seeger, R.; Pople, J. A. *J. Chem. Phys.* **1980**, *72*, 650.
(37) McLean, A. D.; Chandler, G. S. *J. Chem. Phys.* **1980**, *72*, 5639.
(38) Foresman, J. B.; Head-Gordon, M.; Pople, J. A.; Frisch, M. J. *J. Phys. Chem.* **1992**, *96*, 135.
(39) Dooley, R.; Allen, G.; Pamidighantam, S. Computational Chemistry Grid: Production Cyberinfrastructure for Computational Chemistry; *Proceedings of the 13th Annual Mardi Gras Conference*, Baton Rouge, LA2005.
(40) Milfeld, K.; Guiang, C.; Pamidighantam, S.; Giuliani, J. Cluster Computing through an Application-Oriented Computational Chemistry Grid; *Proceedings of the 2005 Linux Clusters: The HPC Revolution*; 2005.
(41) Herzberg, G. *Molecular Spectra and Molecular Strucuture*; Van Nostrand-Reinhold: New York, 1996; Vol. III.
(42) Mulliken, R. S. *J. Chem. Phys.* **1955**, *23*, 1997.
(43) Wilson, E. B. *Phys. Rev.* **1934**, *45*, 0706.
(44) Müller, C. W.; Newby, J. J.; Liu, C.-P.; Zwier, T. S. In preparation, 2008.
(45) Syage, J. A.; Aladel, F.; Zewail, A. H. *Chem. Phys. Lett.* **1983**, *103*, 15.
(46) Haas, Y.; Kendler, S.; Zingher, E.; Zuckermann, H.; Zilberg, S. *J. Chem. Phys.* **1995**, *103*, 37.
(47) Sinclair, W. E.; Yu, H.; Phillips, D.; Gordon, R. D.; Hollas, J. M.; Klee, S.; Mellau, G. *J. Phys. Chem.* **1995**, *99*, 4386.
(48) Hopkins, J. B.; Powers, D. E.; Smalley, R. E. *J. Chem. Phys.* **1980**, *72*, 5039.
(49) Hollas, J. M. *High Resolution Spectroscopy*; John Wiley & Sons: Chichester, 1998, p 249.
(50) Sebree, J. A.; Newby, J. J.; Müller, C. W.; Zwier, T. S. Unpublished results.
(51) Hollas, J. M.; Musa, H.; Ridley, T.; Turner, P. H.; Weisenberger, K. H.; Fawcett, V. *J. Mol. Spectrosc.* **1982**, *94*, 437.
(52) Carreira, L. A.; Towns, T. G. *J. Chem. Phys.* **1975**, *63*, 5283.
(53) Müller, C.; Klöppel-Riech, M.; Schröder, F.; Schroeder, J.; Troe, J. *J. Phys. Chem. A* **2006**, *110*, 5017.
(54) Lewis, J. D.; Malloy, T. B.; Chao, T. H.; Laane, J. *J. Mol. Struct.* **1972**, *12*, 427.
(55) Nelder, J. A.; Mead, R. *Computer J.* **1965**, *7*, 308d.
(56) Pitzer, K. S. *J. Chem. Phys.* **1946**, *14*, 239.
(57) Wong, B. M.; Thom, R. L.; Field, R. W. *J. Phys. Chem. A* **2006**, *110*, 7406.
(58) Peng, C. Y.; Ayala, P. Y.; Schlegel, H. B.; Frisch, M. J. *J. Comput. Chem.* **1996**, *17*, 49.
(59) Peng, C. Y.; Schlegel, H. B. *Isr. J. Chem.* **1993**, *33*, 449.
(60) Dian, B. C.; Clarkson, J. R.; Zwier, T. S. *Science* **2004**, *303*, 1169.
(61) Clarkson, J. R.; Dian, B. C.; Moriggi, L.; DeFusco, A.; McCarthy, V.; Jordan, K. D.; Zwier, T. S. *J. Chem. Phys.* **2005**, *122*, 214311.
(62) Clarkson, J. R.; Baquero, E.; Zwier, T. S. *J. Chem. Phys.* **2005**, *122*, 214312.
(63) Clarkson, J. R.; Baquero, E.; Shubert, V. A.; Myshakin, E. M.; Jordan, K. D.; Zwier, T. S. *Science* **2005**, *307*, 1443.
(64) Syage, J. A.; Lambert, W. R.; Felker, P. M.; Zewail, A. H. *Chem. Phys. Lett.* **1982**, *88*, 266.
(65) Troe, J. *Chem. Phys. Lett.* **1985**, *114*, 241.
(66) Felker, P. M.; Zewail, A. H. *J. Phys. Chem.* **1985**, *89*, 5402.
(67) Zwier, T. S.; Carrasquillo, M. E.; Levy, D. H. *J. Chem. Phys.* **1983**, *78*, 5493.
(68) Amirav, A.; Jortner, J. *Chem. Phys. Lett.* **1983**, *95*, 295.
(69) Khundkar, L. R.; Marcus, R. A.; Zewail, A. H. *J. Phys. Chem.* **1983**, *87*, 2473.
(70) Schroeder, J.; Schwarzer, D.; Troe, J.; Voβ, F. *J. Chem. Phys.* **1990**, *93*, 2393.
(71) Meyer, A.; Schroeder, J.; Troe, J. *J. Phys. Chem. A* **1999**, *103*, 10528.
(72) Syage, J. A.; Felker, P. M.; Zewail, A. H. *J. Chem. Phys.* **1984**, *81*, 4706.
(73) Schulz, K.; Hofmann, J.; Zimmermann, G. *Lieb. Ann. Recueil* **1997**, 2535.
(74) Hofmann, J.; Schulz, K.; Altmann, A.; Findeisen, M.; Zimmermann, G. *Lieb. Ann. Recueil* **1997**, 2541.
(75) Schulz, K.; Hofmann, J.; Zimmermann, G. *Eur. J. Org. Chem.* **1999**, 3407.
(76) Schulz, K.; Hofmann, J.; Findeisen, M.; Zimmermann, G. *Eur. J. Org. Chem.* **1998**, 2135.

JP803254D